Linear and non-linear optical properties of PVA-Ag/Coumarin Nanocomposites

T.Y. Elrasasi *, M.A. Attallah, N.M. Shash, M.G. El-Shaarawy

Department of physics, Faculty of Science, Benha University,
Benha, Egypt.

The Polyvinyl alcohol (PVA)-Ag/Coumarin nanocomposite films with various Coumarin concentrations have been prepared and analyzed. The optical properties and dispersion parameters have been determined. The PVA semicrystalline nature has been ensured by using X-ray Diffraction (XRD). The crystallinity degree decreases with the rise in Coumarin concentration. Scanning electron microscope (SEM) images show that the Ag nanoparticles are distributed all over the surface. Increasing the concentration of Coumarin in PVA-Ag nanocomposites leads to an increase in refractive index, absorption coefficient, and Urbach energy. It also results in a significant decrease in both the energy band gap and the relaxation time. The optical conductivity and dielectric constant were enhanced as well, with the concentration of Coumarin rising. Wemple–Di Domenico single oscillator model has been utilized to calculate the nonlinear optical properties. It was evident that with the rise in Coumarin concentration, the values of nonlinear optical properties n_2, $x^{(1)}$, and $x^{(3)}$ have increased. As a result, the PVA-Ag/30 wt.% Coumarin's good optical characteristics make it ideal for optical applications.

1. Introduction

Sensors, optical filters, plasmonic devices, imaging, medicine, photovoltaic devices, optical switching devices, communication field, and magnetic storage media, for example, are electronic applications that depend mainly upon polymer metallic nanoparticle composite materials [1-2]. The optical material applications are still in their developmental phase, so it is of great importance to provide a new material with unique features [3]. The main objective beyond the evaluation of the optoelectronic materials is to enhance some parameters such as the linear refractive index, optical band gap, third-order nonlinear susceptibility, etc. [4-5]. Since the nonlinear optical features play a key role in modern photonics technology, such as the

development of ultra-short technology pulses, ultrafast switching, managing the frequency spectrum of laser light, and all-optical signal processing. The suitability of a material for these device applications needs a large magnitude of the third-order nonlinear optical susceptibility. Optical nonlinearities are fundamentally weak, as they are governed by photon_ photon interactions enabled by materials though they can be strengthened in material environments that provide mechanisms for field enhancement. Such an increased effective nonlinear optical response can be achieved through plasmonic effects. Such effects arise from coherent oscillations of conduction electrons near the surface of noble metal structures. Recent studies have proved that Ag can also be considered a possible material for plasmonic devices. The enhancement of these parameters can be achieved by altering the nature of the fillers, the size of the embedded particles, and their spread in the matrix of the polymer [6]. Nanoparticle metals (e.g. Fe, Al, Au, Cu, and Ag), oxides of metal (NiO, Al_2O_3, SiO_2, PbO_2, and Fe_2O_3), different nanoparticles (e.g. NaI, CO, HgS, and NaI), semiconductors, carbon nanotubes, and magnetic nanoparticles have been utilized as an additive material in the polymer matrix to enhance its properties [7-26]. Polyvinyl alcohol (PVA) is the most applicable host material for different nanoparticles with its unique physical features represented in high transmittance, non-corrosive nature, chemical resistance, thermostability, high mechanical strength, and easy processability, and high surface area [27-30]. Abdullah et [31] reported that by adding HgS to the PVA matrix the energy bang gap decreased from (6.27 - 4.8) eV. Nouh et al [22] reported that the radiation of IR laser improves the optical energy band gap of PVA/Pd nanoparticles. Rashad [13] clarified that adding Fe_2O_3 within the PVA matrix increases the crystallinity degree, thus increasing the optical band gap. Ahmed et al [19] showed that optical conductivity and dielectric constants increase by increasing the concentration of silicon carbide nanoparticles in PVA/CaO nanocomposites. Ghanipour et al [1] show that the refractive index, crystallinity, and the Braggs planes number in the PVA matrix have been significantly decreased by Ag nanoparticle doping. Chahal et al [32] stated that the presence of Ag in the form of nanoparticles has been confirmed by the surface Plasmon resonance in the PVA/Ag nanocomposites

absorption spectrum around 425 nm. Elshamy [33] has stated that the PVA/Ag nanocomposites film absorption peak has a redshift when the Ag nanoparticle size decreases. Many kinds of literature and researchers have given a special interest in Ag nanoparticles owing to their excellent electrical and optical properties [34]. So it has been used on a wide scale in many applications such as catalysis, magnetic shielding, microelectronics, and others [35]. On the other side, Coumarin dye is considered one of the most active dyes due to its unique structure features including low toxicity, excellent light stability, good solubility, large Stokes shift, and its beneficial optical properties [36]. Coumarin dye is made up of two rings (lactone and benzene) connected. These two rings have either a π-system conjugated or a structure of double bonds [37]. It should be remembered that this π-system conjugated enhances the exchange of electrons between Coumarin and PVA [38, 39]. Despite a large amount of research on improving the PVA/Ag nanocomposite optical properties has been stated, the door is still open for enhancing the PVA/Ag nanocomposites' optical properties to fulling the different applications desires. So introducing PVA-Ag/Coumarin nanocomposites for promising applications and enhancing their structure and optical properties is the aim of this work.

2. Experimental

2.1. Materials

Polyvinyl alcohol ($-CH_2CH(OH)_n$- 87 - 89 % purity) was brought from Alfa Aesar Chemicals, silver nitrate ($AgNO_3$, 99 % purity), and Coumarin ($C_9H_6O_2$), were brought from Sigma-Aldrich For Chemicals.

2.2. PVA-Ag nanocomposites fabrication

PVA/Ag films have been prepared by in situ chemical reduction by solution casting techniques as shown in our paper [56].

2.3. PVA-Ag/Coumarin nanocomposites fabrication

The solution of Coumarin dye prepared by solving 0.8 gm/400 ml deionized water with continuous stirring for one hour at room temperature was added to fabricated PVA/Ag nanocomposites with (0, 4, 8, 12, 16, 30) wt. %.

2.4. Measurements

To confirm the formation of Coumarin dye in PVA, the prepared films with a thickness of 0.1 mm were characterized by using a UV/VIS spectrophotometer (JANEWAY 6405 UV/VIS spectrophotometer) at a wavelength range of 300-900 nm. X-ray diffraction (XRD) X-ray- D/Max 2200 V- Rigaku- Japan at room temperature with CuKα (λ = 0. 15406 nm) radiation has been used to examine the crystallinity of the prepared nanocomposites. Scanning electron microscopy (SEM) has been done by (Quanta 250 FEG) working at voltage 5-30 KV to monitor the implanting of Ag inside the PVA matrix. Fourier transform infrared spectroscopy (FTIR) was done with (Thermo Scientific Nicolet iS10) at the wavenumbers range between 400-4000 cm^{-1}.

3. Results

PVA-Ag/Coumarin dye nano-composites XRD patterns are depicted in Fig. 1. For all the samples, the notable broad peak has been observed at 2θ=20∘, which describes the semi-crystalline PVA polymer's region, [40]. With the rise in Coumarin concentration, this peak intensity has decreased, which signs the reduction in the nano-composite films' crystallinity. The interaction between the nano-composite (PVA-Ag) and the Coumarin dye is responsible for this reduction in crystallization. This suggests a rise in nano-composite disordering behavior [41]. Also, X-ray diffraction patterns showed two other peaks (see the inset in Fig. 1) for the zero Coumarin sample at 2θ=28.5∘ and 32.1∘ characterized for (210) and (122) respectively for the FCC structure of silver with interplanar spacing calculated from Bragg's law d=0.279 nm. This peak intensity decreases as the amount of Coumarin dye in the nano-composite increases which demonstrates the role of Coumarin in damaging planes of crystallization and boosting the amorphous regions of the nano-composite.
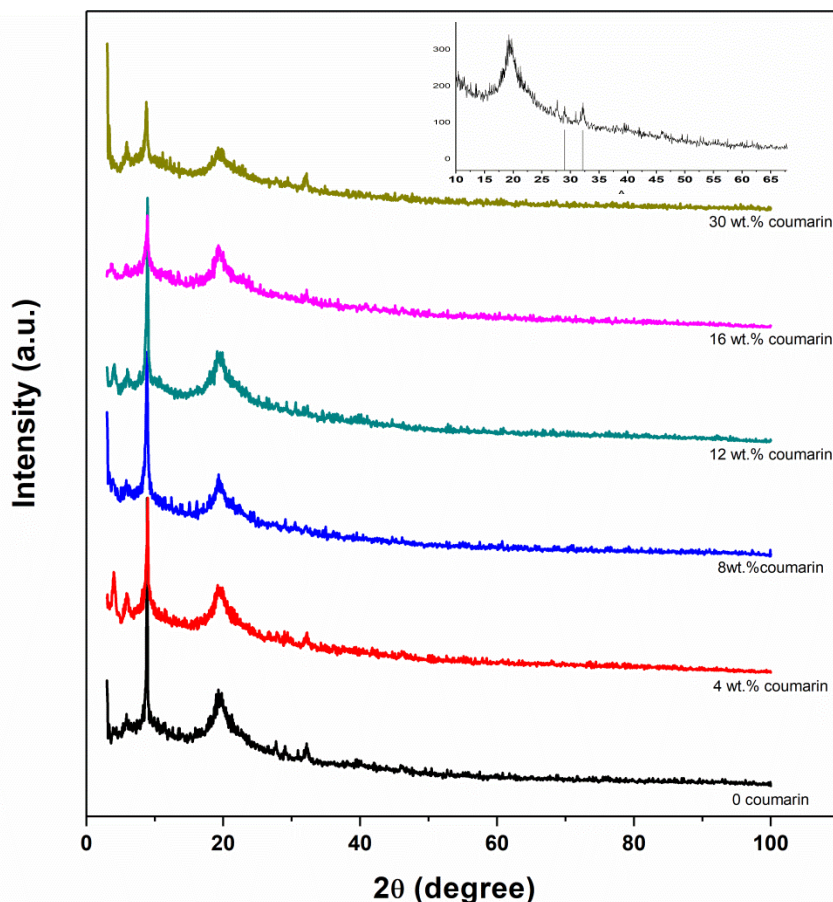
FIGURE 1 XRD of PVA-Ag/Coumarin nanocomposite films. The inset focus on the peaks around 40°.

FT-IR spectra of PVA-Ag/Coumarin dye nano-composite are depicted in Figure 2. For the zero Coumarin sample, some absorption bands at wavenumbers 3610, 2920, 1750, and 1480 cm^{-1} are observed [42,43]. The peak of vibrational at 3610 cm^{-1} is attributed to the stretching of O-H, while the band at 2920 cm^{-1} is related to the C-H stretching. The peak of absorption present at 1750 cm^{-1} is assigned to the C=O stretching and the band at 1480 cm-1 is assigned to the C-H bend of CH$_2$ group. Moreover, the vibrational peaks observed in 1130-650 cm^{-1} could be indicated to Ag-O, owing to the interaction through the Ag+ ion and the PVA polymer. It can be noticed that the same spectra were observed for all the samples with different concentrations of Coumarin, but the intensity of the absorption peaks at 500 - 1100 cm^{-1} increased as the Coumarin concentration dye increased [44]. This may be because of the defects caused by the interaction between the PVA-Ag and Coumarin dye charge transfer. Most of the detected peaks are tabulated in Table 1.
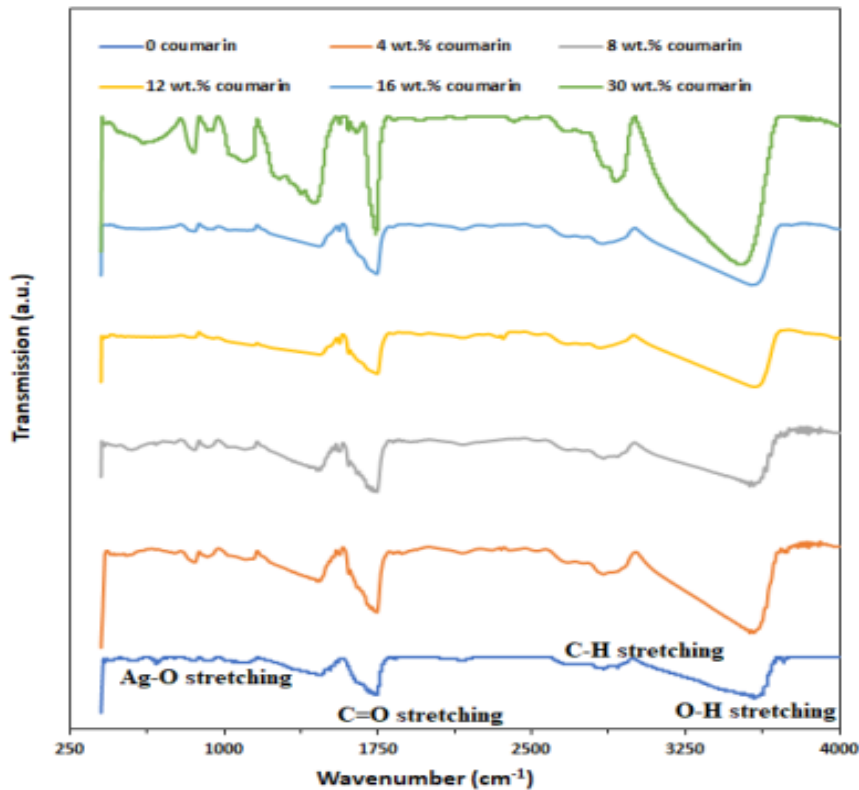
FIGURE 2 FT-IR of PVA-Ag / Coumarin nanocomposite films.

Table 1 Chemical Bonds from FT-IR of PVA-Ag/Coumarin nano composites.

Band assignment	Wavenumbers(cm^{-1})					
	0 wt.% Coumarin	4 wt.% Coumarin	8 wt.% Coumarin	12 wt.% Coumarin	16 wt.% Coumarin	30 wt.% Coumarin
OH stretching	3610	3580	3580	3590	3590	3520
CH stretching	2920	2860	2860	2830	2850	2920
C=O stretching	1750	1750	1740	1750	1750	1740
Symmetric bending of CH_2	1480	1470	1470	1480	1460	1450
Ag-O	1000	996	989	912	984	1210

To study the morphology of the surface and detect the nanocomposite elements, SEM and EDX analyses have been handled. Figure 3(a-c) illustrates the SEM and the EDX of the PVA-Ag/Coumarin dye nano-composite. One can see that Ag nanoparticles with a spherical shape were arranged uniformly. But at high concentrations of Coumarin, Ag

nanoparticles have been agglomerated and formed some clusters on the surface. It could be related to the PVA-Ag/ Coumarin interaction. In the PVA host matrix, EDX has verified the perfect quantities maintenance of silver. As shown, (Ag, O, and C) were observed at energies (3.2, 0.45, and, 0.3 KeV) which represent the nanocomposite contents.
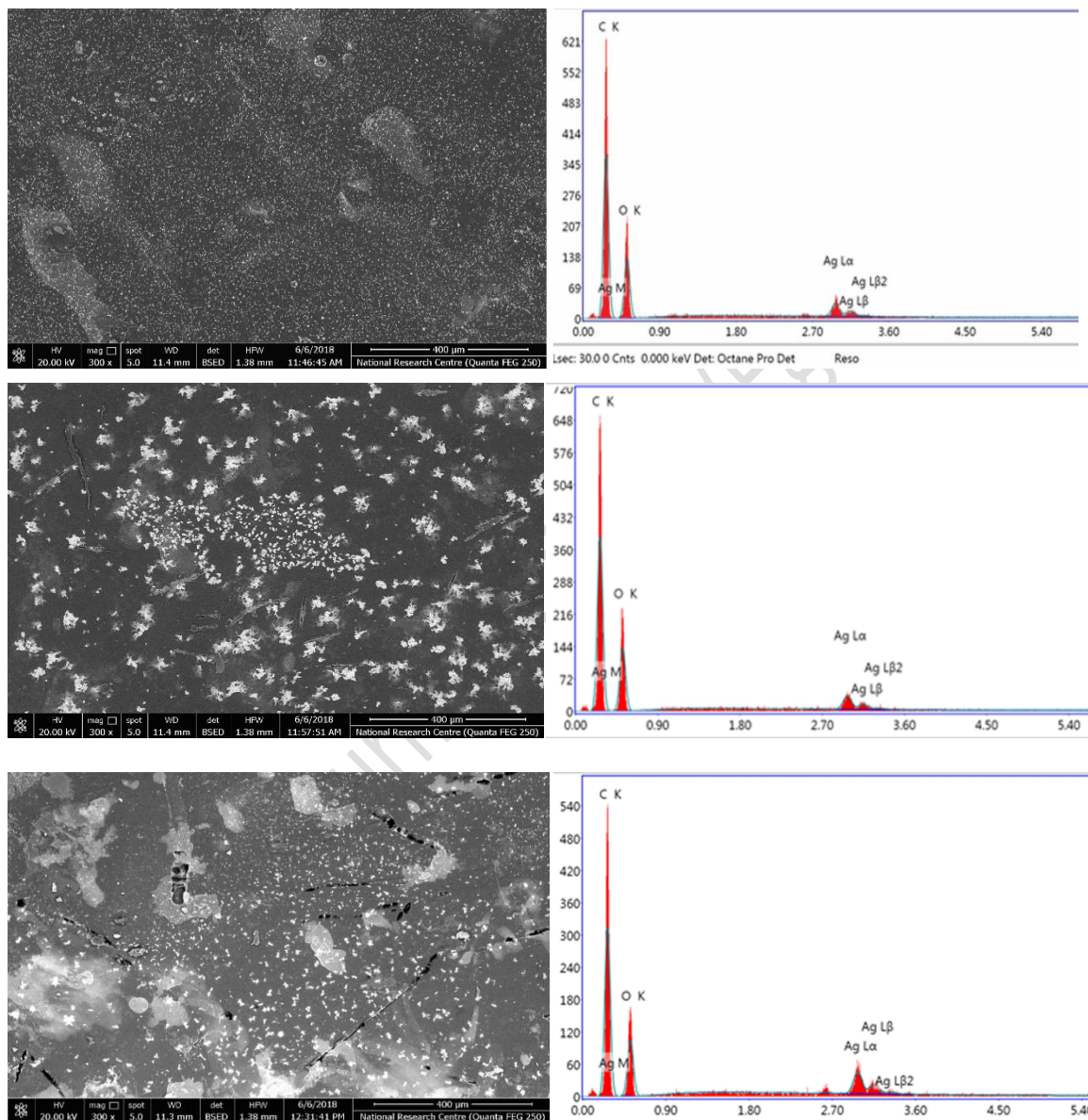

FIGURE 3 SEM images and EDX of PVA-Ag / Coumarin at different concentrations (a) PVA-Ag (b) 8 wt. % Coumarin (c) 30 wt. % Coumarin.

Uv-visible measurement

Fig.4a depicted the absorption spectra of the PVA-Ag/Coumarin dye nano-composites. As a result of Ag formation on the nano-scale, an SPR

peak at λ= 428 nm was realized for PVA-Ag composites in the visible regions [45- 47]. The SPR peak for spherical silver nanoparticles produced from chitosan [48], PNA [49], and natural rubber [50] host polymers was also observed in the same region by other researchers. With the rise of Coumarin concentration, this peak intensity increases due to the exceed in the Ag nanoparticles number as a result of the chemical bonding formation between PVA/Ag and Coumarin dye as revealed in FTIR spectra. Also, it is observed that a redshift in the SPR band position by increasing the Coumarin concentration has appeared. This shift is related to the increase in Ag nanoparticle size (which is confirmed in SEM). These results agree with previous studies stating that the Ag nanoparticle SPR band location embedded in the matrix of polymer shifts to a longer wavelength [49]. This behavior assures the Coumarin role in the Ag nanoparticles formation.

The PVA-Ag/Coumarin dye nanocomposites film transmission spectra are shown in Fig. 4b, which clearly shows the transmission as a narrow band of about 432 nm. It is noticeable that, with an increase in Coumarin concentration, the intensity of this band decreases because the Ag nanoparticle size changes due to the agglomeration in the polymer matrix. This qualified it to be used as a bandpass filter around a certain wavelength via the right selection of polymer matrix, spices of embedded nano-particles, and their size distribution. In the UV region, the change in the transmission spectra is due to the band gap of PVA. For full analysis, the reflection of the incident spectra from the prepared samples has been calculated and plotted in Fig. 4.c.

In Practice, the optical absorption coefficient (α) can be determined from the optical absorbance by [15]:

$$\alpha = \left(\frac{2.303 \times A}{d}\right) \tag{1}$$

where A =log (I/I$_0$), where I and I$_0$ are the transmitted and the incident beam intensities respectively, and d is the film thickness.
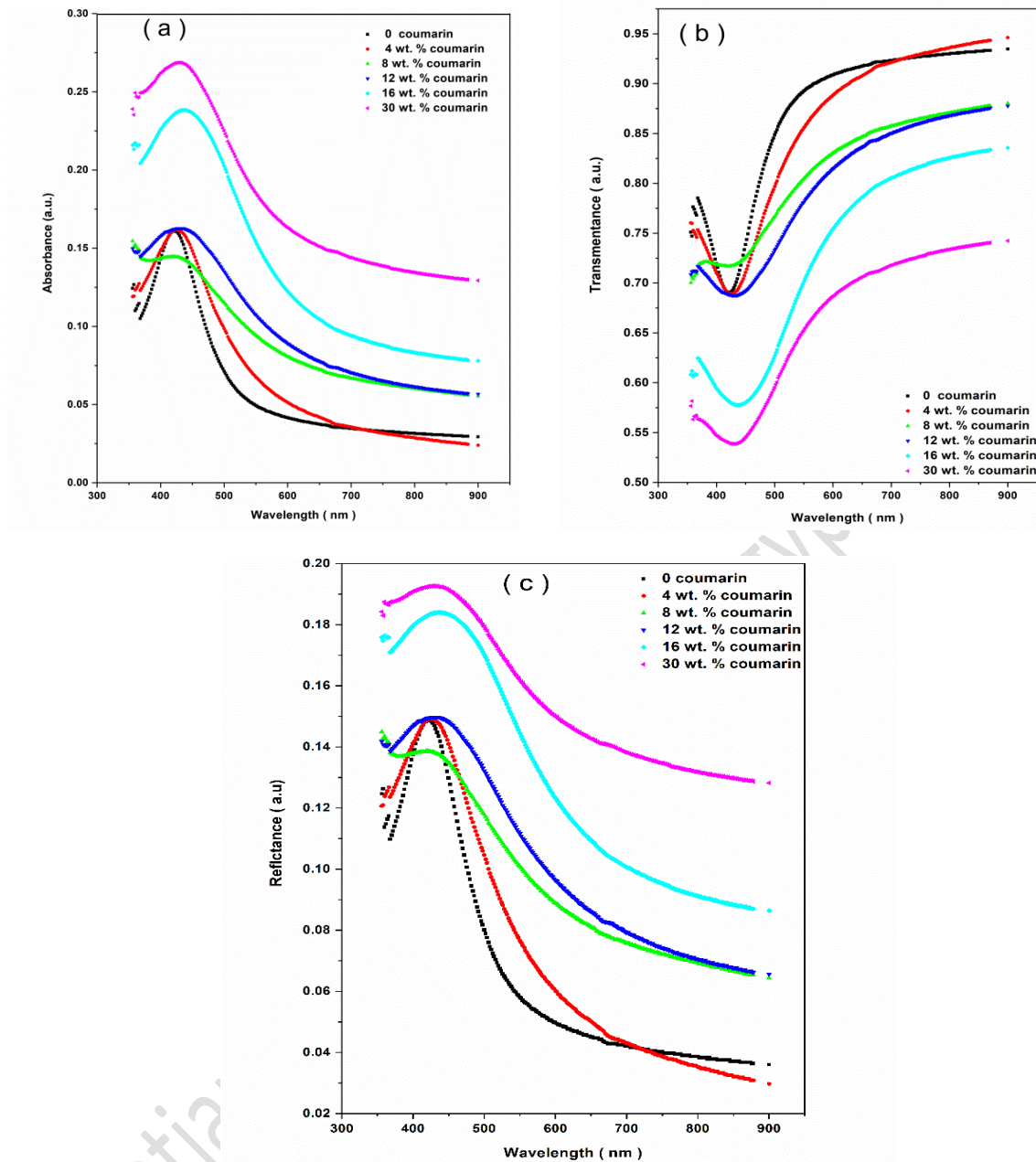
FIGURE 4 (a) The Uv-vis absorption spectra, (b) Transmission spectra, and (c) reflection spectra of PVA –Ag/Coumarin nanocomposite films.

The absorption coefficient (α) spectral behavior for the PVA-Ag/Coumarin dye nanocomposites films is shown in Figure 5a. At low energies, the absorption coefficient of PVA-Ag/Coumarin nanocomposites films is low. This is due to the energy of the incident photon energy isn't enough to transmit the electrons from the valance band to the conduction band [19]. While at high energies, the incident photon energy is sufficient to excite an electron to high levels, so the absorption coefficient increases. The

absorption coefficient of nanocomposites increases with increasing concentrations of Coumarin. This is because the number of charge carriers increases.

The extinction coefficient (k) is given by the equation [51]:

$$k = \frac{\alpha\lambda}{4\pi} \qquad (2)$$

The wavelength dependence of the extinction coefficient (k) is illustrated in Figure 5b. In the UV region, the extinction coefficients were high and then decreased sharply with increasing the wavelength. This is due to the high-energy incident photon in the UV spectrum region being enough to excite the electrons from the valance band to the conduction band [26]. This indicates an energy reduction lost, which means that the extinction coefficient decreases. It is also seen that the extinction coefficient (k) increases with rising concentrations of Coumarin. This is attributed to the absorption of surface Plasmon [1]. The films refractive index (n) was determined by: [32]

$$n = \frac{(1+R)}{(1-R)} + \sqrt{\frac{4R}{(1-R)^2} - k^2} \qquad (3)$$
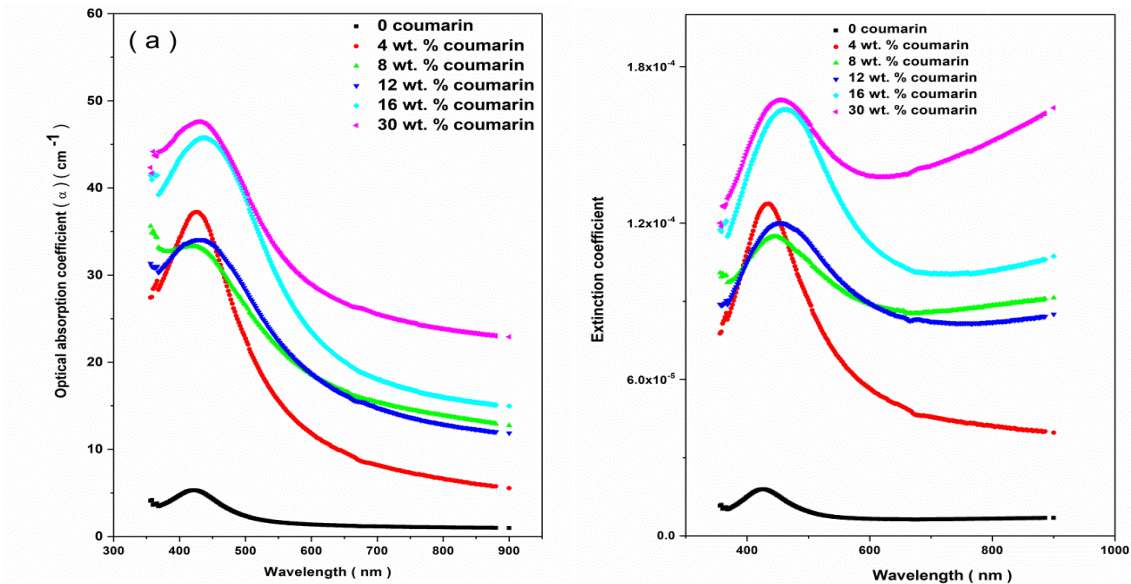

FIGURE 5 (a) Optical absorption coefficient of PVA-Ag /Coumarin nanocomposite films. (b) The extinction coefficient of PVA-Ag / Coumarin nanocomposite films.

The dependence of the refractive index of PVA-Ag/Coumarin dye nanocomposites on the wavelength is depicted in Figure 6. In the visible region (400 - 600 nm), the refractive index decreases as the wavelength increases. However, the refractive index is essentially constant at higher wavelengths (700 - 900 nm). The peak occurring for the samples at wavelengths between 400 and 450 nm is due to the electronic transition from bonding to antibonding molecular orbital. The refractive index increases with increasing the Coumarin dye concentration. Increasing the refractive index is an indication of nanocomposite high density, which results in a decrease in the inter-atomic spacing. This is due to (a) the intermolecular hydrogen bonding between the Coumarin dye and the OH groups of the PVA polymer increasing the packing density [1]. (b) Doping Coumarin in the polymer matrix can destroy the polymer chain order and rise the amorphous (as confirmed by XRD). The amorphous domains' presence prompts the interference of light phenomenon throughout the polymer matrix resulting in the noticed increase in n values [32].
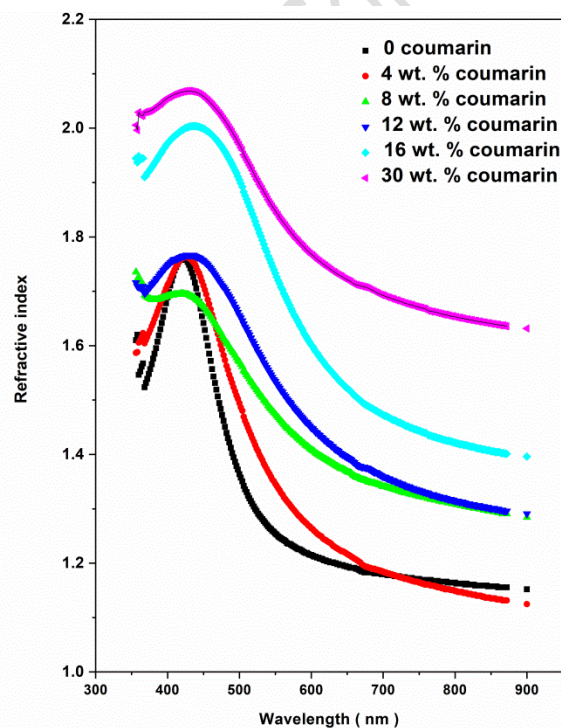

FIGURE 6 Refractive index of PVA-Ag/Coumarin nanocomposite films.

The refractive index dispersion can be investigated by the Wemple-DiDomenico single oscillator model [14]:

$$n^2 = 1 + \frac{E_d E_0}{[E_0{}^2 - (h\upsilon)^2]} \tag{4}$$

where E_d is the dispersion energy and E_0 is the single-oscillator energy. From equation 4, when the $h\upsilon$ goes to zero, then

$$n_0 = \sqrt{\left(1 + \frac{E_d}{E_0}\right)} \tag{5}$$

where n_0 is the static refractive index. By fitting eq.(4) as depicted in Figure 7.a for $\lambda > 400$ nm, the values of E_0 and E_d have been determined and given in Table 2. It seems that the E_0 and E_d values increase by increasing the concentration of Coumarin. The rise in E_0 values are due to the defects in the nanocomposites [15]. The rise in E_0 values are strong evidence for the modification of the international band gap structure by adding coumarin. The rise E_d values because of the increase of the anion strength of the dielectric medium. Subsequently, the PVA-Ag steward is more interested in retaining the electrons in their outward layer [52]. This shows an increase in the charge transfer between PVA-Ag and Coumarin, as well as an increase in the degree of disorder in nanocomposites. According to the following equations,

$$x^{(1)} = E_d/4\pi E_0 \tag{6}$$

$$x^{(3)} = 6.82 \times 10^{-15} (E_d/E_0)^4 \tag{7}$$

$$n_2 = 12\pi\, x^{(3)}/n_0 \tag{8}$$

where $x^{(1)}$, $x^{(3)}$, and n_2 is defined in [26]. Table 2 presents the estimated values of $x^{(1)}$, $x^{(3)}$ and n_2. From the table, one can see that, $x^{(1)}, x^{(3)}$ and n_2 depend on the coumarin concentration as well as on the presence of Ag nanoparticles, which has a strong effect on the $x^{(3)}$ values and hence on the refractive index n_2.

Table 2 The optical dispersion parameters of PVA-Ag/Coumarin nano composites.

Sample wt.%	E_0 (ev)	E_d (ev)	n_0	$\chi^{(1)} \times 10^{-3}$	$\chi^{(3)} \times 10^{-17}$	$n_2 \times 10^{-15}$
0	3.08	0.81	1.12	21	3.3	1.1
4	2.91	0.70	1.11	19	2.4	0.8
8	3.34	1.9	1.25	45	74	22
12	3.23	1.89	1.26	46	81	24
16	3.20	2.62	1.34	65	310	86
30	3.75	5.48	1.56	116	3110	746

Above the absorption edge, the refractive index dispersion given by [53]:

$$\frac{n_\infty^2 - 1}{n^2 - 1} = 1 - \left(\frac{\lambda_0}{\lambda}\right)^2 \tag{9}$$

where n_∞ is the refractive index at an indefinite wavelength, λ_0 is the average wavelength of the interband oscillator. Figure 7b shows the relation between $(n^2 - 1)^{-1}$ versus λ^{-2}. Table 3 includes the values of n_∞ and λ_0 for the prepared samples. It was observed that with increasing the Coumarin concentration, the n_∞ and λ_0 values increases; this is possibly ascribed to the rise in the packing density, and also the increase in amorphous lead to an increase in n_∞. Equation 9 can also be written as, [54]:

$$n^2 - 1 = \frac{S_0 \lambda_0^2}{\left(1 - \left(\frac{\lambda_0}{\lambda}\right)^2\right)} \tag{10}$$

where the average oscillator strength is S_0, and equal to:

$$S_0 = \frac{n_\infty^2 - 1}{\lambda_0^2} \tag{11}$$

The obtained value of S_0 for the samples are presented in Table 3. It is obvious that as the Coumarin concentration increases, S_0 increases. This is attributed to the complexation between Coumarin dye and matrix of polymer which results in the n values changes. According to this study, the optical properties of these nanocomposites have been controlled by the Coumarin addition. These parameter measurements help in the designing and manufacture of such nanocomposites for use in optoelectronic applications.
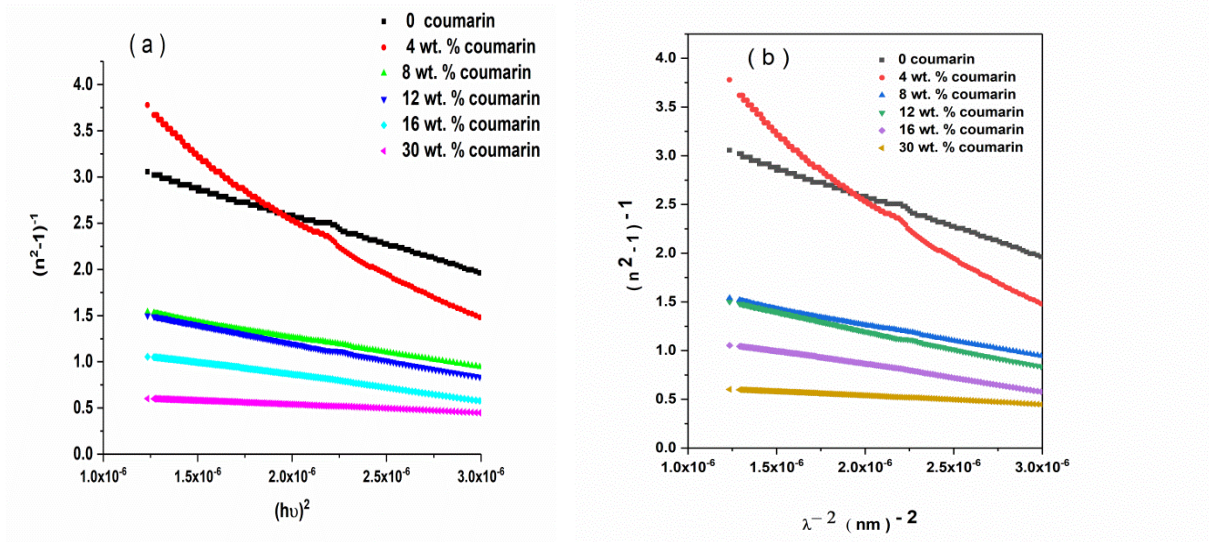
FIGURE 7 (a) Plots of $(n^2 - 1)^{-1}$ vs.$(h\nu)^2$ of PVA-Ag / coumarin nanocomposite films. (b) Plots of $(n^2 - 1)^{-1}$ vs.$(\lambda)^{-2}$ of PVA-Ag / Coumarin nanocomposite films.

Table 3 dispersion parameters of PVA-Ag/Coumarin nanocomposites

Sample wt.%	n_∞	λ_0 (nm)	$S_0 \times 10^{-6}$ $(nm)^{-2}$	ε_∞	(N/ $m^* 10^{56}$) ($kg^{-1} m^{-3}$)	(ω_p $\times 10^{14}$) (sec^{-1})
0	1.12	402.7	1.66	2.62	8.2	9.5
4	1.09	505.2	0.74	2.93	10.2	10
8	1.23	411.8	3	2.96	7.89	8.7
12	1.22	441.2	2.5	3.23	9.38	9.1
16	1.31	437.2	3.7	4.23	13.7	9.6
30	1.55	346.9	11.7	4.42	10.5	8.28

Dielectric constant real (ε_1) and imaginary (ε_2) parts are regarding extinction coefficient (k) as well as the refractive index (n) values [12]

$$\varepsilon_1 = n^2 - k^2 = \varepsilon_\infty - \frac{e^2 N}{4\pi\varepsilon_0 c^2 m^*}\lambda^2 \tag{12}$$

$$\varepsilon_2 = 2nk = \frac{\varepsilon_\infty \omega_p^2}{8\pi c^3 \tau}\lambda^3 \tag{13}$$

where the frequency of plasma resonance is ω_p for free carriers odd sort and is assumed as:

$$\omega_p = \left(\frac{e^2 N}{\varepsilon_0 \varepsilon_\infty m^*}\right)^{\frac{1}{2}} \tag{14}$$

where the electron charge is e, the free space permittivity is ε_0, the residual dielectric constant is ε_∞, the ratio of the free carrier concentration N to the effective mass m^* is N/m^*, the relaxation time is τ and the velocity of light is c. The value of N/m^* and residual dielectric constant ε_∞ could be found by drawing a diagram between the dielectric real part constant ε_1 and λ^2 as shown in Figure 8. From the slopes and intercept N/m^* and ε_∞ values are determined and presented in Table 3. It is noticed that by increasing Coumarin content, both $\frac{N}{m^*}$ and ε_∞ increased and this indicates the rise in free carriers. The plasma resonance frequency ω_p for the free carriers was studied according to Equation 14. From Table 3, one can see that the ω_p increases with raising the concentration of Coumarin that could be attributed to the boost of concentration of carrier N when taking oversight that effective mass m^* is stationary.
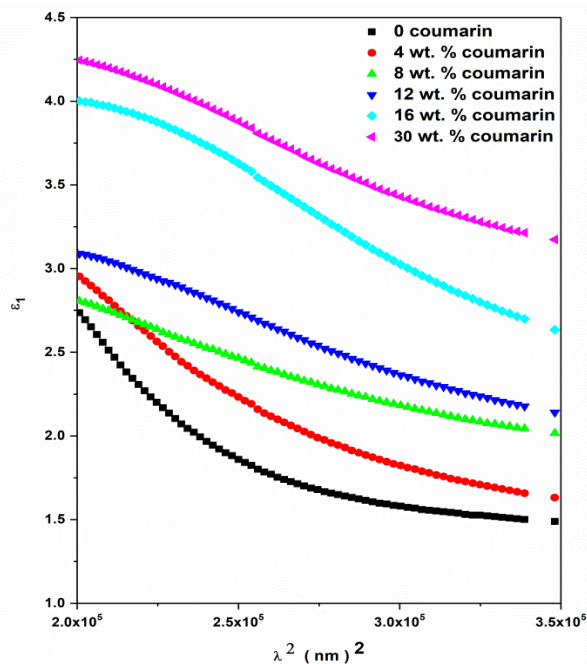

FIGURE 8 Variation of the real part of the dielectric constant with λ^2 of PVA-Ag / Coumarin nanocomposite films.

The reliance of samples' dielectric constants on real and imaginary parts of energy is illustrated in Figure 9 (a-b). As shown in Figure 9. a the ε_1 the value increases by increasing the incident photon energy. This is due to the interaction between electrons in nanocomposites and incident photons. The ε_1 the value increases from 1.8 for (zero Coumarin) sample to 4 for the (30 wt. % Coumarin) sample. This increase ascribed to the predominant association in the nanocomposites that lead to the formation of inter-/intra-molecular hydrogen bonding between silver ion and the hydroxyl (OH) groups is reduced. This in turn led to the higher state density existence and greater accumulated space charge quantities in the nanocomposite resulting in a higher dielectric constant [55].

On the other side, by increasing the energy of the incident photon, the ε_2 values increase. This is owing to the rise in the index of refraction and the excitation coefficient. The dielectric constant real part values are more major than the imaginary part values. The dielectric constant real part is related to the dispersion, whereas the dissipation is represented by the imaginary part.
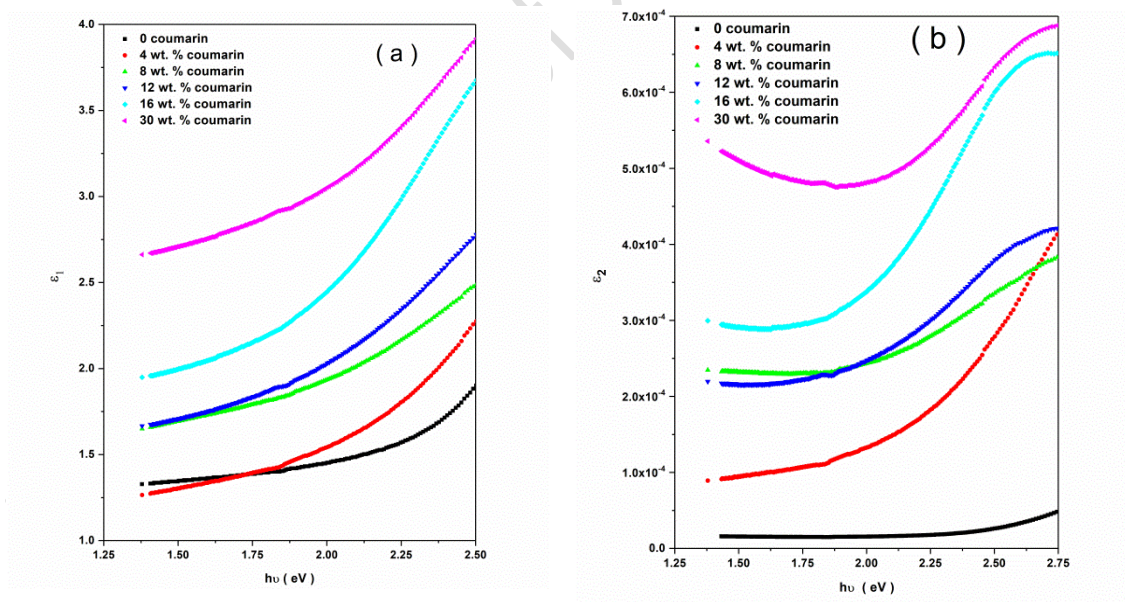

FIGURE 9 Variation of (a) real (b) imaginary part of dielectric constant with hυ of PVA-Ag/Coumarin nanocomposite films.

In Figure10, the reliance of the dielectric relaxation time on the photon energy of the sample is shown. The relaxation time of dipole orientation decrease by increasing the concentration of Coumarin. Such a reduction in the dielectric relaxation time is due to as the concentration of Coumarin increases, the amorphous increase so the chains of polymer are further elastic and can round themselves comparatively extra readily as well as fast [1].
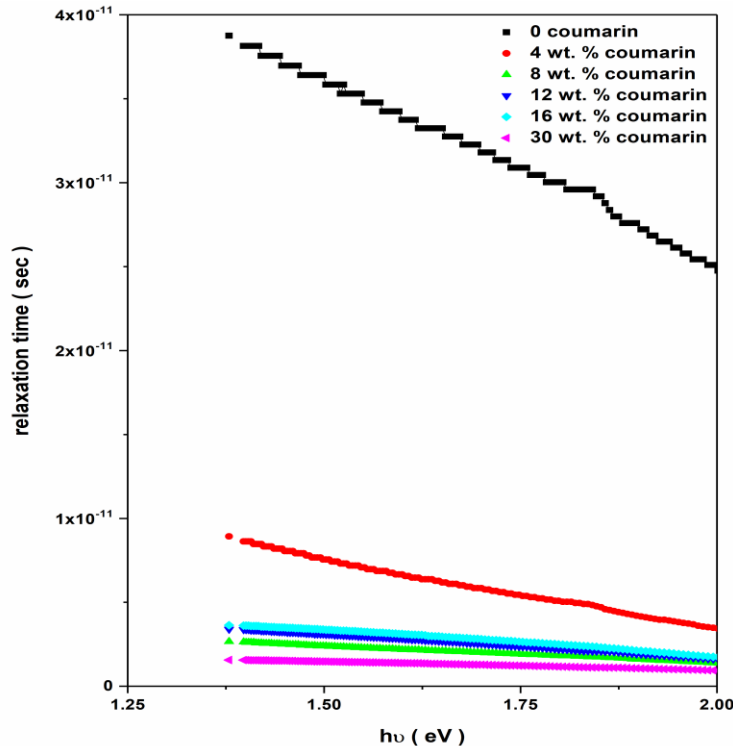

FIGURE 10 The dielectric relaxation time as a function of the photon energy of PVA-Ag/Coumarin nanocomposite films.

Optical conductivity can be calculated by [24]

$$\sigma_{opt} = \frac{\alpha n c}{4\pi} \tag{15}$$

where the optical conductivity is σ_{opt} and the light velocity in the vacuum is c. Figure 11. illustrates the dependence of the optical conductivity on the energy of the incident photon. It is evident that σ_{opt} increases by increasing the energy of the photons. This is because the charge carriers increase as a result of the ability of incident photons to transit electrons from valance to

the conduction band [55]. It is obvious that, with the increase in the concentration of Coumarin, the optical conductivity increase. This is related to (a) the localized tail state formation in the bandgap creates the transition from the valence band to the nearest level states easier. (b) the formation of a charge-transfer complex between Coumarin dye and PVA polymer. (c) the increase in nanocomposites amorphous causes the optical band gap to decrease and the optical conductivity to increase.

The electrical conductivity σ_e, can be calculated according to:

$$\sigma_e = \frac{2\lambda\sigma_{opt}}{\alpha}$$

(16)

The dependence of σ_e on the photon energy $h\nu$ is illustrated in Figure 11b. It can be observed that σ_e decreases by raising the energy of the incident photon. This is due to the increase in absorbance. Also, σ_e increases by increasing Coumarin content. This is attributed to the increase in charge carriers.
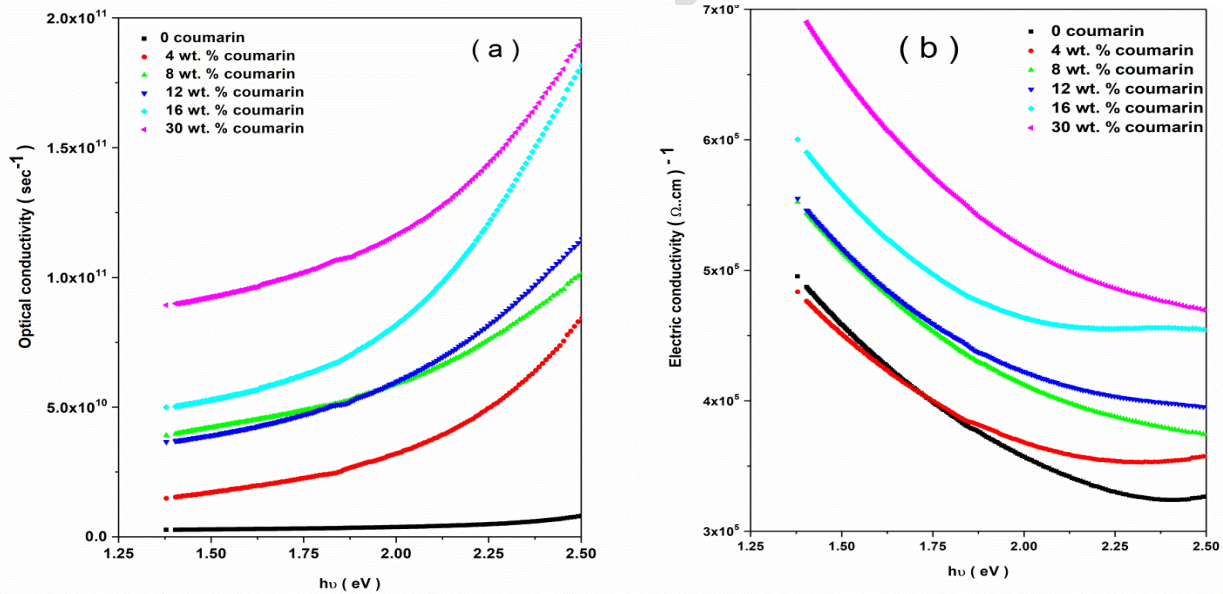

FIGURE 11 (a) Optical (b) electrical conductivity versus hν of PVA-Ag/Coumarin nanocomposite films.

To determine the direct optical bandgap, $(\alpha h\nu)^2$ is plotted verse the photon energy $h\nu$, see Figure 12. The direct optical band gap value is

determined by extrapolating the linear fitted lines on the higher axis in these data points and tabulated in Table 4. It is obvious that the direct bandgap values decrease by doping with Coumarin until it reaches a dopant concentration, 30 wt. %. It is observed that the optical band gap values reduce from 2.5 to 1.9 eV owing to Coumarin's photochemical reaction that reduces the residual Ag+ ions in the metallic silver, this occurs when an electron is released from the chain of PVA [56]. These Ag atoms are responsible for formalizing centralized electronic states in the lowest unoccupied molecular orbital gap and the highest occupied molecular orbit.
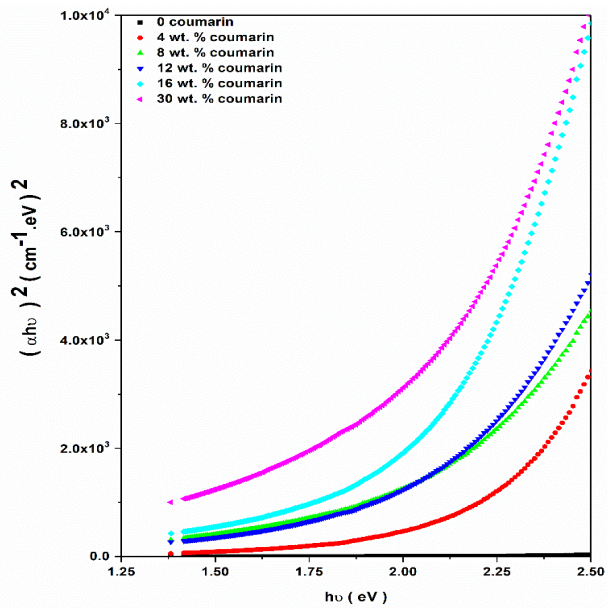

FIGURE 12 Direct bandgap of PVA-Ag/Coumarin nanocomposite films.
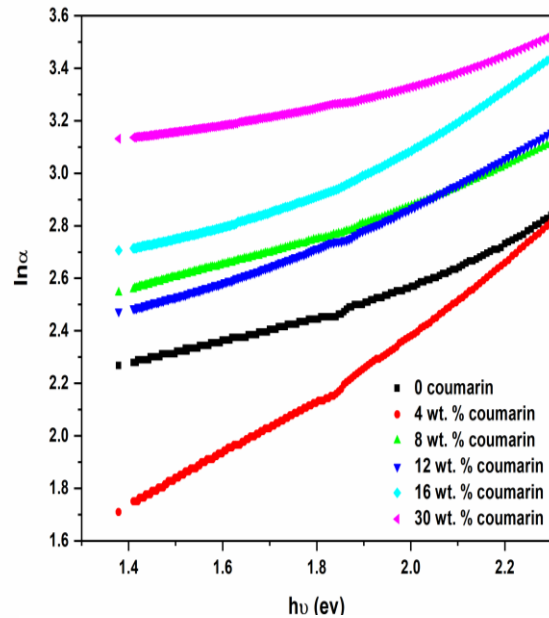
FIGURE 13 Urbach plots of VA-Ag/Coumarin nanocomposite films.

This centralized state is working like a recombination plus trapping center, thus reinforcing the low energy transitions which lead to the detected band gap modulation. The band gap decreases also approves the disorder degree increases in nanocomposites, which could be approved by the localized tail states bandwidth investigation in the forbidden band gap (Urbach energy E_u) employing the subsequent equation [23]

$$\alpha = \alpha_0 \ \exp\left(\frac{h\upsilon}{E_u}\right) \qquad (17)$$

where the coefficient of absorption is α and α_0 is a constant. Fig. 13 illustrates the dependence of Ln (α) on (hυ). The values of E_u were calculated by fitting eq.17 and shown in Table 4. It can be seen that with the increase in coumarin concentrations, the E_u values increase. This indicates that the degree of structural disorder of nanocomposites has increased. Hence, it contributes to the localized states increasing and the optical band gap decreasing. The enhancement in our nanocomposite properties is reported in Table 4. As well as the easy preparation, flexibility are environmentally friendly, and economical. Our nanocomposite shows a high absorbance, high refractive index, high dispersion parameters, narrow transmission band (432 nm), and low energy band gap (1.9 eV), which qualifies it to use in the photovoltaic application, photoelectric diversion, optical communication, bandpass optical filters, optoelectronic application respectively.

Table 4 Optical band gap values and Urbach energy for PVA-Ag/Coumarin nanocomposite films.

Sample (wt.%)	Direct Band Gap (eV)	Urbach energy (ev)
0	2.5	1.78
4	2.4	0.86
8	2.1	1.72
12	2.05	1.38
16	2	1.31
30	1.9	2.56

Conclusion:

The PVA-Ag/Coumarin nanocomposite films have been prepared using a different concentration of Coumarin dye. The XRD patterns assured the existence of the Ag nanoparticles in the nanocomposites. Also, the crystallinity was decreased due to the increase of the disorder and the amorphous in the nanocomposite. Besides, the SEM images proved the presence of Ag in and on the composite surfaces. The optical spectra proved the Coumarin dye effect on the PVA-Ag nanocomposites' optical properties. The refractive index increases with increasing Coumarin concentration and reach the coveted value, which is optimum for better photoelectric diversion rendering. The band tail width increased from 1.7 to 4 eV. The optical conductivity is increased by increasing Coumarin content. So, the results suggested the potential implementation of PVA- Ag/Coumarin nanocomposites films in solar cells and other photovoltaic devices as well as nonlinear optical devices. The optical energy bandgap reduces with growing Coumarin. The narrow transmission band of about 432 nm cement the present nanocomposite films for enforcement as a bandpass for optical filters.

Declaration of Conflicting Interests

The authors declared no potential conflicts of interest concerning the research, authorship, and/or publication of this article.

References:

1. M. Ghanipour, D. Dorranian, Effect of Ag-nanoparticles doped in polyvinyl alcohol on the structural and optical properties of PVA films, J. Nanomater. 2013 (2013) 1–10, https://doi.org/10.1155/2013/897043.
2. P. Pascariu, A. Airinei, M. Grigoras, L. Vacareanu, F. Iacomi, Metal-polymer nanocomposites based on Ni nanoparticles and polythiophene obtained by electrochemical method, Appl. Surf. Sci. 352 (2015) 95–102, https://doi.org/10.1016/j.apsusc.2015.03.063
3. A.L. Stepanov, Optical properties of polymer nanocomposites with functionalized nanoparticles, Polym. Compos. with Funct. Nanoparticles. (2019) 325–355, https://doi.org/10.1016/B978-0-12-814064-2.00010-X
4. K. Waszkowska, O. Krupka, O. Kharchenko, V. Figa, V. Smokal, N. Kutsevol, B. Sahraoui, Influence of ZnO nanoparticles on nonlinear optical properties, Appl. Nanosci. (2020) 1–6, https://doi.org/10.1007/s13204-020-01373-3.
5. A. Ismail, M. Mohammed, E. El-Metwally, Influence of Gamma irradiation on the structural and optical characteristics of Li ion-doped PVA/PVP solid polymer electrolytes, Indian J Phys 93 (2019) 175–183. DOI.org/10.1007/s12648-018-1286-1.

6. H. Mao, J. Feng, X. Ma, Can Wu, X. Zhao, One-dimensional silver nanowires synthesized by self-seeding polyol process. J. Nanopart. Res (2012) 1-15. DOI 10.1007/s11051-012-0887-4.

7. F. Naseri, D. Dorranian, Effect of aluminum nanoparticles on the linear and nonlinear optical properties of PVA, Opt. Quant. Electron. 49 (2017) 4, https://doi. org/10.1007/s11082-016-0839-9.

8. S.B. Aziz, S. Hussein, A.M. Hussein, S.R. Saeed, Optical characteristics of polystyrene based solid polymer composites: effect of metallic copper powder, Int. J. Med. 2013 (2013), 123657, https://doi.org/10.1155/2013/123657.

9. K. Lance Kelly, Eduardo Coronado, A. Lin Lin Zhao, G.C. Schatz, The optical properties of metal nanoparticles: the influence of size, shape, and dielectric environment, J. Phys. Chem. 107 (2003) 668–677. https://doi.org/10.1021/ JP026731Y.

10. A. Zihlif, A.S. Faduos, G. Ragosta, Optoelectrical properties of polymer composite: polystyrene-containing iron particles, J. Thermoplast. Compos. Mater. 26 (2012) 1180–1191, https://doi.org/10.1177/0892705712437394.

11. F. Ahmad, M. Hassan, Structure and Physical Properties of Al2O3 Nanofillers Embedded in Poly(Vinyl Alcohol), POLYMER COMPOSITES 5 (2018) 1-7, DOI 10.1002/pc.24937.

12. S. Aziz, A. Hassan, S. Mohammed, W. Karim , M. Kadir , H. Tajuddin and N. Chan, Structural and Optical Characteristics of PVA:C-Dot Composites: Tuning the Absorption of Ultra Violet (UV) Region, Nanomaterials 9 (2019) 216, doi:10.3390/nano9020216

13. M. Rashad, Tuning optical properties of polyvinyl alcohol doped with different metal oxide nanoparticles, Optical Materials 105 (2020) 109857, https://doi.org/10.1016/j.optmat.2020.109857.

14. M. Banerjee, A. Jain, G.S. Mukherjee, Microstructural and optical properties of polyvinyl alcohol/manganese chloride composite film, Polym. Compos. 40 (2019) E765–E775, https://doi.org/10.1002/pc.25017.

15. M. Mohamed, M. Abdel Kader, Effect of excess oxygen content within different nano-oxide additives on the structural and optical properties of PVA/PEG blend, Applied Physics A 125 (2019) 209-220, https://doi.org/10.1007/s00339-019-2492-1.

16. F. Ali, Structural and optical characterization of [(PVA:PVP)-Cu2+] composite films for promising semiconducting polymer devices, Journal of Molecular Structure 1189 (2019) 352-359, https://doi.org/10.1016/j.molstruc.2019.04.014 0.

17. S.Choudhary, Characterization of amorphous silica nanofiller effect on the structural, morphological, optical, thermal, dielectric and electrical properties of PVA–PVP blend based polymer nanocomposites for their flexible nanodielectric applications, Journal of Materials Science: Materials in Electronics 29 (2018) 10517–10534 https://doi.org/10.1007/s10854-018-9116-y.

18. N. Deghiedy, S. El-Sayed, Evaluation of the structural and optical characters of PVA/PVP blended films, Optical Material 100 (2020)109667, https://doi.org/10.1016/j.optmat.2020.109667 R.

19. H. Ahmed, H. Abduljalil · A. Hashim, Structural, Optical and Electronic Properties of Novel (PVA–MgO)/SiC Nanocomposites Films for Humidity Sensors, Transactions on Electrical and Electronic Materials (2019) 20:218–232 https://doi.org/10.1007/s42341-019-00111-z.

20. V. Viswanath, S. Nair, G. Subodh, C. Muneera, Emission features, surface morphology and optical limiting properties of semiconducting Toluidine Blue O dye poly(vinyl alcohol) nanocomposite architecture, SN Applied Sciences (2019) 1:43 | https://doi.org/10.1007/s42452-018-0043-6.

21. G.Shetty , V. Crastab,, R. Kumar, R. Kb , R. Bairy , P. Patile, Promising PVA/TiO2, CuO filled nanocomposites for electrical and third order nonlinear optical applications, Optical Material 95 (2020) 109218
https://doi.org/10.1016/j.optmat.2019.109218.

22. S. Nouh , K. Benthami, Gamma Induced Changes in the Structure and Optical Properties of ZnS/PVA Nanocomposite, JOURNAL OF VINYL AND ADDITIVE TECHNOLOGY—2019, DOI 10.1002/vnl.21689.

23. T. Solimana, S. Vshivkov, Effect of Fe nanoparticles on the structure and optical properties of polyvinyl alcohol nanocomposite films, Journal of Non-Crystalline Solids 519 (2019) 119452, https://doi.org/10.1016/j.jnoncrysol.2019.05.028.

24. T. Soliman, A. Abouhaswa, Synthesis and structural of Cd0.5Zn0.5F2O4 nanoparticles and its infuence on the structure and optical properties of polyvinyl alcohol flms, Journal of Materials Science: Materials in Electronics (2020)
https://doi.org/10.1007/s10854-020-03512-6 .

25. T. Soliman, S. Vshivkov, S. Elkalashy, Structural, thermal, and linear optical properties of SiO2 nanoparticles dispersed in polyvinyl alcohol nanocomposite films, Polymer Composites 41 (2020) 3340–3350.
DOI: 10.1002/pc.25623.

26. T. Soliman, S. Vshivkov, S. Elkalashy, Structural, linear and nonlinear optical properties of Ni nanoparticles – Polyvinyl alcohol nanocomposite films for optoelectronic applications, Optical Materials 107 (2020) 110037
https://doi.org/10.1016/j.optmat.2020.110037.

27. Z.H. Mbhele, M.G. Salemane, C.G.C.E. Van Sittert, J.M. Nedeljković, V. Djoković, A.S. Luyt, Fabrication and Characterization of Silver-Polyvinyl Alcohol Nanocomposites. Chem. Mater. 15 (2003) 5019–5024.
https://doi.org/10.1021/cm034505a.

28. C. Li, W. Zhang, B. Zhao, M. Liang, C. Lu, Preparation, characterization and thermal behavior of poly(vinyl alcohol)/organic montmorillonite nanocomposites through solid-state shear pan-milling. J. Therm Anal Calorim 103 (2011) 205–212.
DOI 10.1007/s10973-010-0975-6.

29. Q. Cheng, S. Wang, T.G. Rials, S.H. Lee, Physical and mechanical properties of polyvinyl alcohol and polypropylene composite materials reinforced with fibril aggregates isolated from regenerated cellulose fibers. Cellulose 14 (2007) 593–602.
DOI 10.1007/s10570-007-9141-0.

30. Y. Tauran, A. Brioude, A.W. Coleman, M. Rhimi, B. Kim, Molecular recognition by gold, silver and copper nanoparticles. World J. Biol. Chem. 4 (2013) 35.
DOI: 10.4331/wjbc.v4.i3.35 · Source: PubMed.

31. O. G. Abdullah1, Y. A.K. Salman, S. A. Saleem, In-situ synthesis of PVA/HgS Nanocomposites films and tuning Optical properties, Phys. Mater. Chem. 3 (2015) 18–24.
DOI: 10.12691/pmc-3-2-1.

32. R.P. Chahal, S. Mahendia, A.K. Tomar, S. Kumar, UV irradiated PVA–Ag nanocomposites for optical applications. Appl. Surf. Sci. 343 (2015) 160–165. https://doi.org/10.1016/j.apsusc.2015.03.074.

33. A.G. El-Shamy, Composite (PVA/Cu nano) films: Two yield points, embedding mechanism and thermal properties, Progress in Organic Coating 127 (2019) 252- 259. https: //doi.org/10.1016/j.porgcoat.2018.11.024.

34. H. Mao, J. Feng, X. Ma, Can Wu, X. Zhao, One-dimensional silver nanowires synthesized by self-seeding polyol process. J. Nanopart. Res (2012) 1-15. DOI 10.1007/s11051-012-0887-4.

35. [35] M. Liu, P. G, Preparation and optical properties of silver chalcogenide coated gold nanorods. J. Mater. Chem. 16 (2006) 3942–3945. DOI: 10.1039/b607106f.

36. [36] P.S. Jogi, J. Meshram, J. Sheikh, T.Hadda, Synthesis, biopharmaceutical characterization, and antimicrobial study of novel azo dye of 7- hydroxy-4-methyl coumarin. Med. Chem. Res. 22 (2013) 4202–4210. DOI 10.1007/s00044-012-0421-3.

37. P. K. Jain, H. Joshi, Coumarin: Chemical and Pharmacological Profile. J. Appl. Pharma. Sci. 6 (2012) 236-240. DOI: 10.7324/JAPS.2012.2643.

38. Y. Yang, J. Zou, H. Rong, G.D. Qian, Z.y. wang, M.q. wang, Influence of various coumarin dye on the laser performance of laser dye co-doped into ORMOSILs. Appl. Phys. B 86 (2007) 309–313. DOI: 10.1007/s00340-006-2462-0.

39. [39] K.G. Weng, Y.L. Yuan, Brazilian, Synthesis and evaluation of coumarin derivatives against human lung cancer cell lines. J. Med. Bio. Res. 50 (2017) 1-6. http://dx.doi.org/10.1590/1414-431X20176455.

40. R.P. Chahal, S. Mahendia, A.K. Tomar, S. Kumar, c-Irradiated PVA/Ag nanocomposite films: Materials for optical applications. J. Alloys. Compd. 538 (2012) 212–219. http://dx.doi.org/10.1016/j.jallcom.2012.05.085.

41. W. Attia, K.M.A. El-kader, the optical and mechanical properties of PVA-Ag nanocomposite films. J. Alloys. Compd. 590 (2014) 309–312. http://dx.doi.org/10.1016/j.jallcom.2013.11.203.

42. M.Abdelaziz, E.M Abderazek, Effect of dopant mixture on structural, optical and electron spin resonance properties of polyvinyl alcohol. Phys. B 390 (2007) 1-9. DOI:10.1016/j.physb.2006.07.067.

43. B.Suo, X.Su, J.Wu, D.Chen, A.Wang, and Z.Guo, Poly (vinyl alcohol) thin film filled with CdSe–ZnS quantum dots: Fabrication, characterization and optical properties. Mater.Chem. Phy. 119 (2010) 237-242. Doi:10.1016/j.matchemphys.2009.08.054

44. A.S.Kutesenko and V.M.Granchak, Photochemical synthesis of silver Nanoparticle in Polyvinyl alcohol matercies. Theo. Exp. Chem. 45 (2009) 313-318. DOI: 10.1007/s11237-009-9099-0.

45. [A.G. El-Shamy, An efficient removal of methylene blue dye by adsorption onto carbon dot @ zinc peroxide embedded poly vinyl alcohol (PVA/CZnO2) nano-composite: A novel Reusable adsorbent, polymer 202 (2020). https://doi.org/10.1016/j.polymer.2020.122565.

46. A.G. El-Shamy, Synthesis of new magnesium peroxide (MgO2) nano-rods for pollutant dye removal and antibacterial applications, Mater. Chem. Phys. 243 (2020), https://doi.org/10.1016/j.matchemphys.2020.122640.

47. A.G. El-Shamy, H.S.S. Zayied, New polyvinyl alcohol/carbon quantum dots (PVA/CQDs) nanocomposite films: Structural, optical and catalysis properties, Synth. Met. 259 (2020), https://doi.org/10.1016/j.synthmet.2019.116218.

48. S. Aziz , O. Abdullah , D.Saber , M. Rasheed , H. Ahmed, Investigation of Metallic Silver Nanoparticles through UV-Vis and Optical Micrograph Techniques, Int. J. Electrochem. Sci., 12 (2017) 363 – 373, doi: 10.20964/2017.01.22.

49. M. Rehana, A. Nadab , T. Khattab , N.Abdelwahede , A. El-Kheir, Development of multifunctional polyacrylonitrile/silver nanocomposite films: Antimicrobial activity, catalytic activity, electrical conductivity, UV protection and SERS-active sensor, j. matters technol . 9 (2 0 2 0) 9380–9394,
https://doi.org/10.1016/j.jmrt.2020.05.079.

50. C. Danna, D. Cavalcante, A. Gomes, L. Silva, E. Yoshihara, I.Román, L. Salmazo, M.Pérez, R.roca,and A. Job, Silver Nanoparticles Embedded in Natural Rubber Films: Synthesis, Characterization, and Evaluation of In Vitro Toxicity, Journal of Nanomaterials (2016) 1-8 http://dx.doi.org/10.1155/2016/2368630.

51. V. Ghorbani, M. Ghanipour, D. Dorranian, Effect of TiO2/Au nanocomposite on the optical properties of PVA film, Opt. Quant. Electron. 48 (2016) 61,
https://doi.org/ 10.1007/s11082-015-0335-7.

52. A. Elwhab B. Alwany, O. M. Samir, Mohammed A. Algradee1, M. M. Hafith, M. A. Abdel-Rahim, Investigation of the Effect of Film Thickness and Heat Treatment on the Optical Properties of TeSeSn Thin Films. World J. Cond. Ma.r Phy. 5 (2015) 220-231. http://dx.doi.org/10.1016/j.apsusc.2005.10.040.

53. I.S. Saini, J. Roza, N. Chandak, S. Aggarwal, P.K. Sharma, A.Sharma, Tailoring of electrical, optical and structural properties of PVA by addition of Ag nanoparticles. Mater. chem. Phys. 139 (2013) 802-810.
https://doi.org/10.1016/j.matchemphys.2013.02.035.

54. F.Yakuphanoglu, A.Cukurovali, I.Yilmaz, Determination, and analysis of the dispersive optical constants of some organic thin films. Phys. B. 351 (2004) 53-58.
https://doi.org/10.1016/j.physb.2004.05.010.

55. F. Muhammad, S. Aziz, S. Hussein, Effect of the dopant salt on the optical parameters of PVA:NaNO3 solid polymer electrolyte, J Mater Sci: Mater Electron 26 (2015) 521–529.
DOI 10.1007/s10854-014-2430-0

56. M.A. Attallah, T.Y. Elrasasi, N.M. Shash, M.G. El-Shaarawy, F. El-Tantawy , A. G. El-Shamy, New hybrid nanocomposite based on (PVA-Ag-Coumarin) for high sensitive photodiode device, Materials Science in Semiconductor Processing 126 (2021), https://doi.org/10.1016/j.mssp.2020.105653.